PLASMONIC PROPERTIES AND OPTICAL ACTIVITY OF A THREE-DIMENSIONAL SIX-BLADE WINDMILL NANOSTRUCTURE[**]

Zhaohua Wang[*], Liqing Ren, Hanying Wang

College of Energy Engineering, Yulin University,
719000, Yu Lin, China; e-mail: wangzhaohua841102@163.com

Two exchangeable LSPR modes with different coupling field are observed in calculating magnetic field intensity in accordance with adjusting geometrical parameters. Compared with planar nanostructures, three-dimensional windmills show stronger optical activity, and the maximum value of the asymmetry g-factor was 0.6. The numerical simulation results in this paper also contain the optimal geometrical parameters to achieve the best circular dichroism effect at different resonance modes. The results give a contribution to the design of novel chiral optical nanostructures.

Keywords: *surface plasmon resonance, surface-enhanced spectroscopy, chirality, optical activity.*

ПЛАЗМОННЫЕ СВОЙСТВА И ОПТИЧЕСКАЯ АКТИВНОСТЬ ТРЕХМЕРНОЙ НАНОСТРУКТУРЫ ТИПА ШЕСТИЛОПАСТНОЙ “ВЕТРЯНОЙ МЕЛЬНИЦЫ”

Zh. Wang[*], L. Ren, H. Wang

УДК 535.375.5;620.3

Энергетический колледж Юлинского университета,
719000, Юй Лин, Китай; e-mail: wangzhaohua841102@163.com

(Поступила 4 апреля 2017)

При расчете напряженности магнитного поля в зависимости от заданных геометрических параметров наблюдаются два сменяемых друг друга режима локализованного поверхностного плазмонного резонанса с различными связывающими полями. По сравнению с плоскими наноструктурами наноструктуры типа трехмерных ветряных мельниц проявляют более сильную оптическую активность, максимальное значение g-фактора асимметрии достигает 0.6. Численное моделирование также дает оптимальные геометрические параметры для достижения максимального кругового дихроизма при различных резонансных режимах. Полученные результаты имеют значение для разработки новых хиральных оптических наноструктур.

Ключевые слова: *поверхностный плазмонный резонанс, поверхностно-усиленная спектроскопия КР, хиральность, оптическая активность.*

Introduction. Chirality refers to the geometrical property that the original microscopic or macroscopic structure cannot be brought to congruence with its mirror image [1–3]. As the illumination of circularly polarized electromagnetic waves, which are also chiral, between chiral structure and light, the interaction leads to different optical response in transmittance, reflection, and absorption. Meanwhile, this is called the circular dichroism (CD) effect [4–6]. In this way, chirality can be applied to obtain essential structural information by their specific optical response to the optical field with circular polarization. It reinvigorated the traditional field of molecular structure identification method, which requires breaking the objects detected [7–9]. Mostly, CD is identified as the difference in absorption of left circularly polarized (LCP) and right circularly polarized (RCP) light. Artificial metal nanostructures with strong CD effects have also attracted a large

[**] Full text is published in JAS V. 86, No. 3 (http://springer.com/10812) and in electronic version of ZhPS V. 86, No. 3 (http://www.elibrary.ru/title_about.asp?id=7318; sales@elibrary.ru).

amount of attention and is employed to characterizing organic and biological molecules in common [10–13]. The optical activity of artificial metal nanostructures can be extremely enhanced by the surface plasmons (SPs) [14, 15] which is the collective oscillations of electrons confined to metal-dielectric interfaces [16–19]. In the course of the past decades, chiral nanostructures have been researched carefully, and the most straightforward image of chiral configuration is the helix [20–24], which presents broadband optical activity in the near-IR region. Nevertheless, the study and analysis of the helix structure are regarded as a dilemma due to its high production costs and difficultly of fabrication.

For the sake of bridging the gap between high performance optical activity and relatively easy geometry structure, and taking into account the flexible manipulation into consideration, a three-dimensional chiral windmill-shaped nanostructure with adjusting lift-up degree of each blade is designed. Achieving optical activity has been proposed and discussed by utilizing the asymmetry of two-dimensional planar windmill-shaped nanostructure [25, 26]; however, the CD results are not optimal. Optical activity is in the range of the visible and near-infrared spectral range, where three-dimensional (3D) windmill-shaped nanostructure clearly outperforms the planar design by almost two orders of magnitude, accompanying the flexible control of the interaction between individual branches.

In our work, pronounced optical activity enhancement is achieved means of bringing 2D windmill into 3D by the lift-up of one vertex of each blade to different degrees. In the course of this progress, the emergence of two distinct plasma resonant modes is caused by different coupling methods of normally incident LCP and RCP light, and the optical far-field transmittance spectroscopy displays a different response. Both LSPR modes and optical activity greatly rely on the lift-up degree of each blade.

Structure and simulation method. In Fig. 1, the shape and geometry parameters of 2D and 3D windmill nanostructures with different lift-up degrees are illustrated. Each windmill structure is located on the glass substrate and consists of six blades of identical shape and size, each of which is an equilateral triangle with length of sides a = 100 nm, and thickness of each blade h = 10 nm, noting that the distance between each of the two opposite triangles is g = 20 nm. For each blade, one side of the isosceles triangle is fixed, and the opposite vertex is lifted to different degrees θ depicted, as shown in Fig. 1. When rotating along the z axle, n×60° (n = 1, 2, …, n), each windmill nanostructure will coincide with itself.

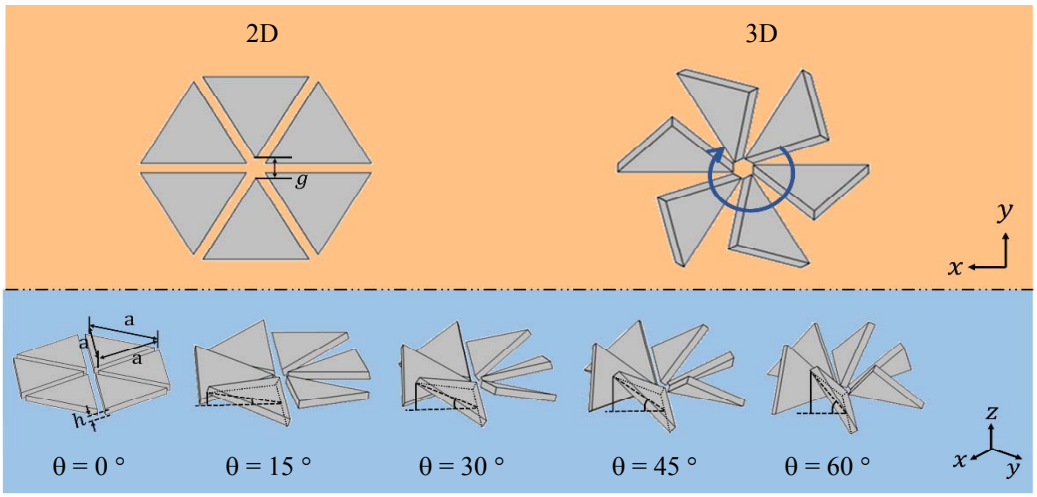

Fig. 1. The geometric shape of 2-dimensional and 3-dimensional windmill nanostructure.

In this study, all structures are modeled with a commercial FEM package (Comsol Multiphysics) for the numerical analysis [27]. The material of the windmills is silver, its parameters were taken from [28], and 3D windmill nanostructures are supported by a glass substrate with n_{glass} = 1.46 and surrounded by air n_{air}= 0. The structure is surrounded by the perfect matching layer which simulates the far field. Ports 1 and 2 are employed to introduce circularly polarized light. Both left (LCP) and right circularly polarized (RCP) light is normally incident along the z axis from the port 1 into the structures and leaves according to port 2. With the coupling between the metal nanostructure and light, the incident energy is taken up, reflected, and transmitted through the structure. In this work, the optical activity of a metal windmill nanostructure is explored by

means of analysis of its transmittance. The *S*-parameters of ports 1 and 2 are calculated to obtain the transmittance. The *S*-parameters are defined as follows:

$$S_{11} = \frac{\int_{\text{port1}}((E_c - E_1)E_1^*)dA_1}{\int_{\text{port1}}(E_1E_1^*)dA_1}, \quad S_{21} = \frac{\int_{\text{port2}}(E_cE_2^*)dA_2}{\int_{\text{port2}}(E_2E_2^*)dA_2},$$

where E_1, E_2 are the electric field patterns on ports 1 and 2, and E_c is the computed electric field. Here, the $|S_{21}|^2$ and $|S_{11}|^2$ are used to calculate the transmittance and reflection of the system.

Under both LCP and RCP light, the optical activity is marked as the difference in transmittances. In this paper, asymmetry of the *g*-factor is defined by following equation [29]:

$$g = (T_{\text{LCP}} - T_{\text{RCP}})/(T_{\text{LCP}} + T_{\text{RCP}}),$$

which is employed to define the difference in transmittance for both LCP and RCP.

Results and discussion. In Fig, 2, the calculated optical far-field transmittance spectroscopy of 2D and 3D (with θ = 60°) structures is depicted. Two distinct LSPR resonance modes are noted at 910 and 1105 nm in the planar nanostructure, and 925 and 985 nm in the 3D windmill structure. Comparing the short wavelength resonance mode of both 2D and 3D windmill nanostructure, the spectral line of the 3D nanostructure with 60° lift-up angle shows narrower spectral width. The spectral position of resonance obviously changed from 2D to 3D structure. All these differences suggest that the two LSPR resonance modes may arise from different coupling pathways between individual blades of a windmill, as explained below.

Figure 2 shows the apparent difference in optical activity of the 2D and 3D nanostructures under normal incident LCP (dark solid line) and RCP (red dot line) light. As for the planar windmill structures with the higher symmetry, the transmittance spectral lines of LCP and RCP are totally aligned, and the different reaction from different polarized light is negligible small. For the 3D structure with lift-up angle 60°, resulting from symmetry reduction, a relatively different transmission intensity occurs for both resonance modes. As for Fig. 2b, the short wavelength (925 nm) and long wavelength (985 nm) resonance modes are characterized by LCP and RCP light, respectively. For the resonance at 925 nm, the resonance for LCP light is much stronger than RCP light, and the transmission dip for LCP light is much deeper than for RCP light. At the same time, for 985 nm the resonance for RCP light is considerably stronger than LCP light.

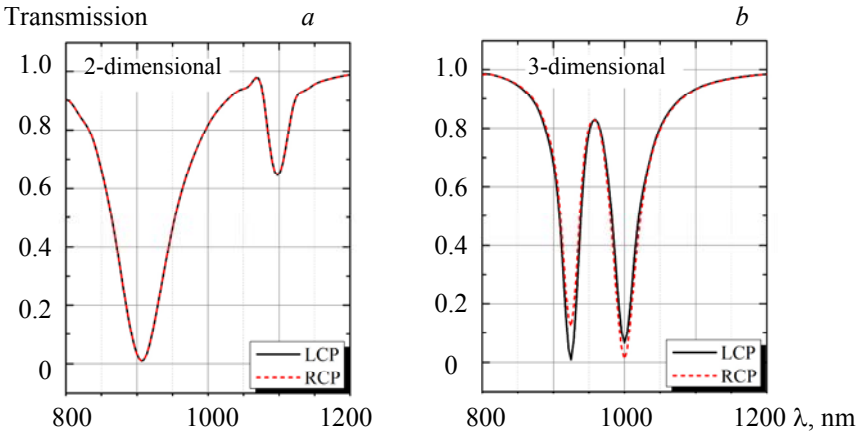

Fig. 2. Transmission of (a) 2-dimensional and (b) 3-dimensional (θ=60°) windmill nanostructure under left circularly polarized (LCP) and right circularly polarized (RCP) light.

The surface current distribution and intensity of the magnetic field at the interface between windmill and substrate at the resonance peaks for LCP and RCP light for planar and 3D (θ = 60°) windmills are demonstrated and analyzed in Fig. 3 and 4 for the sake of understanding the physical mechanism of the optical response for windmill nanostructure. In the graphs of current density, vector arrows point in the direction of current flow, while current amplitude is indicated by the length of the arrow. As for magnetic field, the intensity is indicated by the color bar beside it.

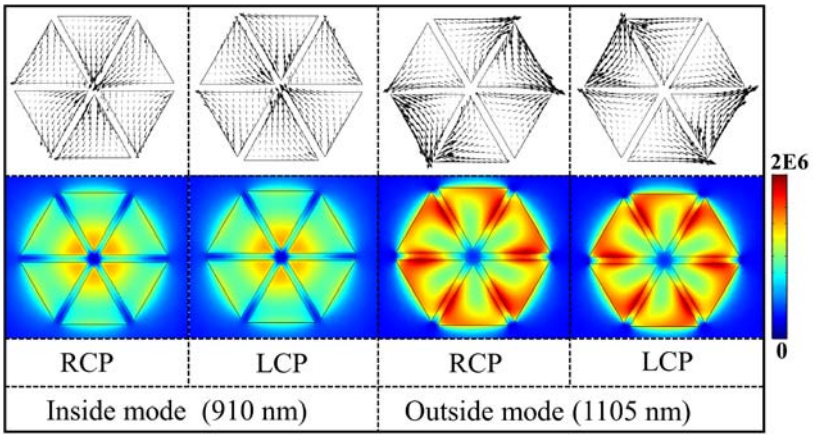

Fig. 3. The surface current density and magnetic field for planar nanostructure at 910 and 1105 nm.

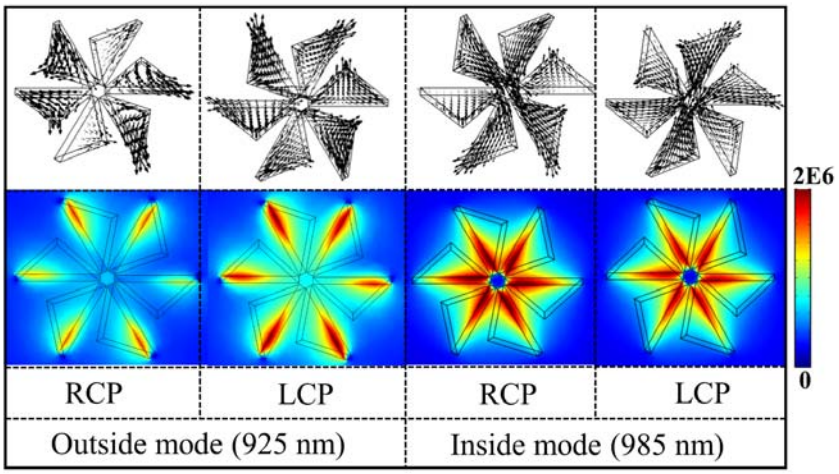

Fig. 4. The surface current density and magnetic field for 3-dimensional windmill nanostructure ($\theta = 60°$) at 925 and 985 nm.

Inside mode and outside mode are used to distinguish the two coupling modes. Inside mode refers to the strong interaction between the inside parts of the blades, as shown in Fig. 2a, which are located at the short-wavelength (910 nm) LSPR mode of transmittance spectroscopy. As shown in Fig. 3, the surface current distribution for a planar nanostructure exhibits collection and enhancement at center, and the intensity of the magnetic field even more obviously points out the central enhancement position. The surface current distribution of the outside mode in Fig. 3 also reveals the enhancement area. For both inside and outside modes, the magnetic field intensity shows no difference for left and right polarized light.

As revealed by far-field transmittance spectroscopy in Fig. 2b, the 3D windmills with 60° lift-up angle presents a different response to LCP and RCP light at the LSPR region. For resonance at 925 nm, the intensity of the magnetic field at the interface of a windmill and a substrate reveals stronger response for LCP light than for RCP light, corresponding to the deeper dip in Fig. 2b at 925 nm, while for the resonance at 985 nm, a windmill at θ=60° shows stronger intensity of the magnetic field for RCP light compared with LCP light excitation. Comparing the intensity of the magnetic field in Fig. 4 with the optical far-field transmittance in Fig. 2b provides an explanation of the difference in optical activity.

It is noteworthy that for a 3D windmill nanostructure, both inside and outside modes still exist although they change the location in the spectra. Outside mode shifts to the blue side of the inside mode, as showed in Fig. 4, and the LSPR mode of 925 nm exhibits enhancement at the outside edge of each blade for both surface current distribution and magnetic field intensity. Meanwhile, for the internal resonance mode, the surface current from a single blade encounter with each other in the field is located close to the center of the

particle, hence the magnetic field is strengthened in the same region. Optical far-field transmittance spectroscopy accompanied by magnetic field intensity at LSPR peaks with gradually growing lift-up angle (θ = 0, 15, 30, 45, and 60°) for LCP light illumination is calculated in order to further investigating the origin of mode-exchanging phenomenon of the exploited plasmonic nanostructure.

As demonstrated Fig. 3, the field of coupling is located close to the central part of the windmill nanostructure, when the lift-up angle is equal to 0°, and the resonance peak is located at the short-wavelength side of the outside mode. When the lift-up angle is improved to 15°, both inside and outside resonance modes expand their enhancement area, which even makes it hard to distinguish them. With further elevating each blade of the windmill nanostructure to 30, 45, and 60°, in contrast to 0°, the outside mode is located at a shorter wavelength than the inside mode, and the two modes are clearly shown by the magnetic field intensity.

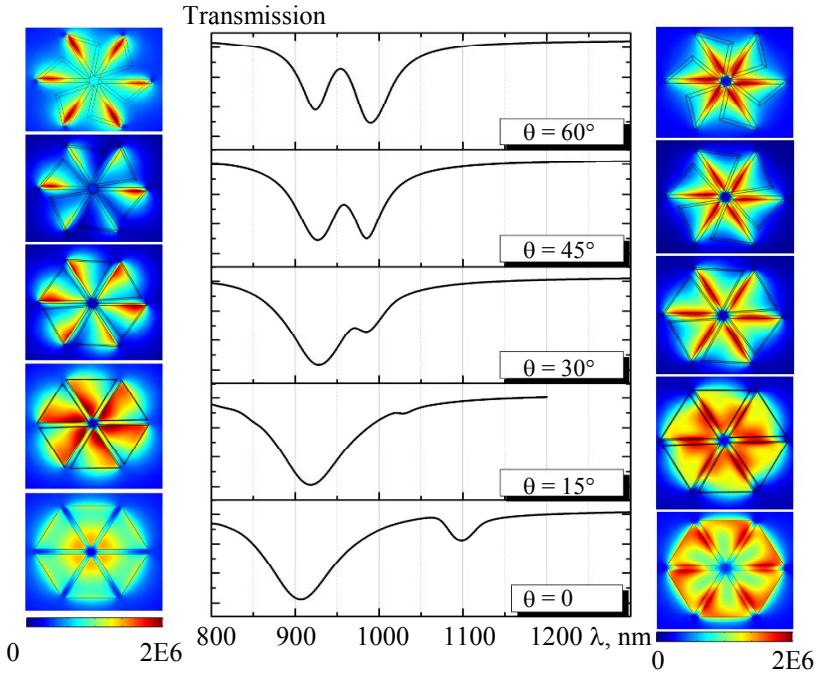

Fig. 5. Transmission and magnetic field for windmill nanostructure with different lift-up angles (θ). The magnetic fields located at left (right) side represents the short (long) wavelength mode of transmission spectra in the same row.

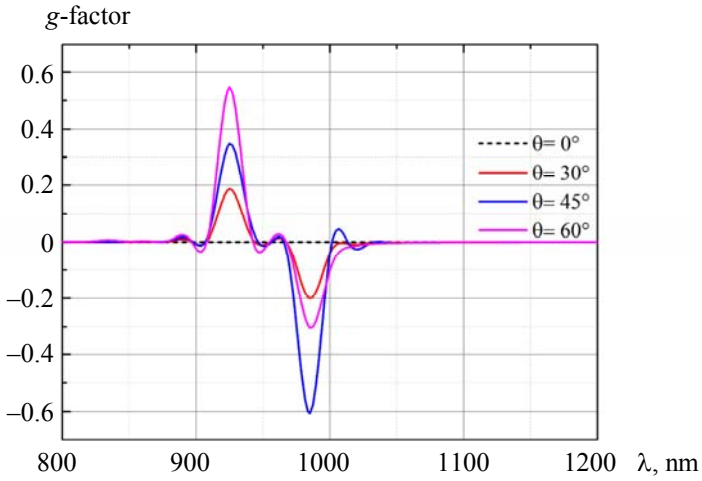

Fig. 6. *g*-Factor of windmill nanostructure with different lift-up angles θ.

The asymmetry *g*-factor is calculated following the equation mentioned before to obtain and manipulate the chiral optical properties of the 3D windmill nanostructures. The dark dot line in Fig. 6 refers to the *g*-factor of a planar windmill nanostructure, which is almost equal to zero for 800–1200 nm. It reveals the absence of optical activity. For a 3D windmill with θ = 30, 45, and 60° (Fig. 6), the two g-factor peaks exist around the wavelength of 925 and 985 nm, which is the location of the outside and inside mode. The adjusting of the lift-up angle from ~30–60°, mainly changes the value of the *g*-factor of the two resonance modes with no influence on the resonance wavelength.

The *g*-factor of the corresponding 3D windmill reaches up to 0.58 for the outside mode at 925 nm and –0.6 for the privileged mode of 985 nm. It should be pointed out that the typical *g*-factor order of magnitude is below 10^{-3} in the majority of cases [20]. Additionally, the spectra of the *g*-factor reveal different signs at two resonances. The value reaches its maximum with the lift-up angle ~60°, hence, the outside edges of the proposed windmill structure exhibits maximum difference for the different polarized light when θ = 60°. In the mode of inside resonance, the field is close to the central part of the windmill, which is susceptible to structural asymmetry and the chirality leads to the changes in the *g*-factor. When θ = 45°, the absolute value of the *g*-factor reaches the maximal value of 0.6 at the inside resonance mode.

Conclusion. A windmill nanostructure is proposed with an adjustable lift-up angle, making it transformable from a planar to a 3D nanostructure. In accordance with detailed analysis associated with transmission, surface current distribution, and magnetic field intensity at the interface, two distinct resonance modes arising from the coupling of the central area and the external boundary of the windmill are observed. Notably, the inside and outside modes exchange their locations by increasing lift-up angle from 0 to 30°. The result of LSPR mode shows strong dependence on geometrical parameters and can be adjusted flexibly. In addition, the optical activity for the 3D windmill (θ = 30–60°) can be tailored to obtain the maximum *g*-factor 1.58 at the outside resonance mode and –1.60 at the inside resonance mode. The windmill nanostructure realizing the maximum *g*-factor at the two modes feature θ = 60 and 45°. The optical activity is highly sensitive to the lift-up degree, so the nanostructure proposed may have strong potential in the fields of biosensors, surface enhanced spectroscopy, and refractive index detection.

Acknowledgment. This work is supported by the Yulin College high-level talent research start fund project (11GK61), Shaanxi Provincial Science and Technology Agency Project (2014K05-11).

REFERENCE

1. G. M. Sherman, *Nature*, **224**, 1108–1110 (1969).
2. S. M. Kelly, T. J. Jess, N. C. Price, *Biochim. Biophys. Acta – Proteins and Proteomics*, **1751**, No. 2, 119–139 (2005).
3. P.-P. Wei, A. B. Tomter, Å. K. Røhr, K. K. Andersson, E. I. Solomon, *Biochemistry*, **45**, No. 47, 14043–14051 (2006).
4. D. L. Jaggard, A. R. Mickelson, C. H. Papas, *Appl. Phys. (Berl.)*, **18**, No. 2, 211–216 (1979).
5. G. D. Fasman, *Circular Dichroism and the Conformational Analysis of Biomolecules*, Springer, New York (2013).
6. A. Guerrero-Martínez, J. L. Alonso-Gómez, B. Auguié, M. M. Cid, L. M. Liz-Marzán, *Nano Today*, **6**, No. 4, 381–400 (2011).
7. Y. Tang, A. E. Cohen, *Science*, **332**, No. 6027, 333–336 (2011).
8. Y. Tang, A. E. Cohen, *Phys. Rev. Lett.*, **104**, No. 16, 163901 (2010).
9. E. Hendry, T. Carpy, J. Johnston, M. Popland, R. V. Mikhaylovskiy, A. J. Lapthorn, S. M. Kelly, L. D. Barron, N. Gadegaard, M. Kadodwala, *Nat. Nanotechnol.*, **5**, No. 11, 783–787 (2010).
10. M. Hentschel, L. Wu, M. Schäferling, P. Bai, E. P. Li, H. Giessen, *ACS Nano*, **6**, No. 11, 10355–10365 (2012).
11. J. M. Slocik, A. O. Govorov, R. R. Naik, *Nano Lett.*, **11**, No. 2, 701–705 (2011).
12. J. Dong, Z. Zhang, H. Zheng, M. Sun, *Nanophotonics*, **4**, No. 1, 472–490 (2015).
13. J. Dong, S. Qu, H. Zheng, Z. Zhang, J. Li, Y. Huo, G. Li, *Sensor. Actuator. B: Chem.*, **191**, 595–599 (2014).
14. N. J. Halas, S. Lal, W. S. Chang, S. Link, P. Nordlander, *Chem. Rev*, **111**, 3913−3961 (2011).
15. N. Verellen, P. Van Dorpe, C. Huang, K. Lodewijks, G. A. Vandenbosch, L. Lagae, V. V. Moshchalkov, *Nano Lett.*, **11**, No. 2, 391–397 (2011).

16. N. A. Abdulrahman, Z. Fan, T. Tonooka, S. M. Kelly, N. Gadegaard, E. Hendry, A. O. Govorov, M. Kadodwala, *Nano Lett.*, **12**, No. 2, 977–983 (2012).
17. K. Konishi, T. Sugimoto, B. Bai, Y. Svirko, and M. Kuwata-Gonokami, *Opt. Express*, **15**, No. 15, 9575–9583 (2007).
18. A. O. Govorov, Z. Fan, P. Hernandez, J. M. Slocik, R. R. Naik, *Nano Lett.*, **10**, No. 4, 1374–1382 (2010).
19. M. Hentschel, M. Schäferling, T. Weiss, N. Liu, H. Giessen, *Nano Lett.*, **12**, No. 5, 2542–2547 (2012).
20. J. K. Gansel, M. Thiel, M. S. Rill, M. Decker, K. Bade, V. Saile, G. V. Freymann, S. Linden, M. Wegener, *Science*, **325**, No. 5947, 1513–1515 (2009).
21. K. A. Bachman, J. J. Peltzer, P. D. Flammer, T. E. Furtak, R. T. Collins, R. E. Hollingsworth, *Opt. Express*, **20**, No. 2, 1308–1319 (2012).
22. Valev, V. K., Smisdom, N., Silhanek, A. V., De Clercq, B., Gillijns, W., Ameloot, M., V. V. Moshchalkov, Verbiest, T. *Nano Lett.*, **9**, No. 11, 3945–3948 (2009).
23. J. Hu, X. Zhao, R. Li, A. Zhu, L. Chen, Y. Lin, B. Cao, X. Zhu, C. Wang, *Opt. Express*, **24**, No. 10, 11023–11032 (2016).
24. J. K. Gansel, M. Latzel, A. Frölich, J. Kaschke, M. Thiel, M. Wegener, *Appl. Phys. Lett.*, **100**, No. 10, 101109 (2012).
25. S. Kaya, *Opt. Mater. Express*, **4**, No. 11, 2332–2339 (2014).
26. K. Dietrich, C. Menzel, D. Lehr, O. Puffky, U. Hübner, T. Pertsch, A. Tünnermann, E. B. Kley, *Appl. Phys. Lett.*, **104**, No. 19, 193107 (2014).
27. C. F. Bohren, D. R. Huffman, *Absorption and Scattering of Light by Small Particles*, Wiley-VCH Verlag GmbH (2008).
28. P. B. Johnson, R W. Christy, *Phys. Rev. B*, **6**, No. 12, 4370 (1972).
29. J. H. Singh, G. Nair, A. Ghosh, A. Ghosh, *Nanoscale*, **5**, No. 16, 7224–7228 (2013).